Wind tunnel study of wake-induced aerodynamics of parallel stay-cables and power conductor cables in a yawed flow

Mohammad Jafaria and Partha P. Sarkar*

Department of Aerospace Engineering, Iowa State University, Ames, IA 50011, USA

(Received October 16, 2019, Revised May 5, 2020, Accepted May 12, 2020)

Abstract. Wake-induced aerodynamics of yawed circular cylinders with smooth and grooved surfaces in a tandem arrangement was studied. This pair of cylinders represent sections of stay-cables with smooth surfaces and high-voltage power conductors with grooved surfaces that are vulnerable to flow-induced structural failure. The study provides some insight for a better understanding of wake-induced loads and galloping problem of bundled cables. All experiments in this study were conducted using a pair of stationary section models of circular cylinders in a wind tunnel subjected to uniform and smooth flow. The aerodynamic force coefficients and vortex-shedding frequency of the downstream model were extracted from the surface pressure distribution. For measurement, polished aluminum tubes were used as smooth cables; and hollow tubes with a helically grooved surface were used as power conductors. The aerodynamic properties of the downstream model were captured at wind speeds of about 6-23 m/s (Reynolds number of 5×10^4 to 2.67×10^5 for smooth cable and 2×10^4 to 1.01×10^5 for grooved cable) and yaw angles ranging from 0° to 45° while the upstream model was fixed at the various spacing between the two model cylinders. The results showed that the Strouhal number of yawed cable is less than the non-yawed case at a given Reynolds number, and its value is smaller than the Strouhal number of a single cable. Additionally, compared to the single smooth cable, it was observed that there was a reduction of drag coefficient of the downstream model, but no change in a drag coefficient of the downstream grooved case in the range of Reynolds number in this study.

Keywords: tandem arrangement; smooth cylinders; grooved cylinders; yawed cable; bundled cables; power conductors

1. Introduction

Flow over twin circular cylinders has been extensively studied in the past (Tsutsui 2012, Zdravkovich 1987, Zdravkovich 1977) due to its wide applications such as heat exchangers, cooling systems, offshore structures, marine risers, buildings, struts, grids, bridge piers, periscopes, chimneys, towers, power transmission lines, and bridge cables (Sumner 2010). The arrangement of twin cylinders depending on the flow direction is classified as tandem, staggered, and side-by-side arrangements. For parallel cylinders, when the fluid flow passes the first cylinder (upstream), the vortex shedding generated by the first cylinder can influence not only itself but also the second cylinder (downstream) by generating unsteady fluid forces leading to vortex- or wake-induced vibration. These flowinduced vibrations can result in fatigue damage or stressinduced failure of the cylindrical structure or its components. Although the characteristics of the flow over single and tandem cylinders (smooth) in normal flow have been widely investigated by using wind tunnel experiments (Wu et al. 1994, Alam et al. 2003, Alam 2014) and numerical simulations (Braun and Awruch 2005, Lin et al.

*Corresponding author, Professor E-mail: ppsarkar@iastate.edu aPh. D.

E-mail: mjafari@iastate.edu

Copyright © 2020 Techno-Press, Ltd. http://www.techno-press.com/journals/was&subpage=7 2016, Wu et al. 2020), the aerodynamics of yawed smooth and yawed grooved cylinders in a tandem arrangement has not been fully studied. Past studies on the single yawed cylinder or cable have shown that an axial flow is produced behind the yawed cylinder in its wake interrupting the communication of vortex shedding from the top and bottom surfaces of the cylinder (Matsumoto et al. 1990, Matsumoto et al. 2010). In this paper, the aerodynamics of yawed smooth and grooved circular cylinders in a tandem arrangement is studied by using a pair of stationary section models of circular cylinders in a wind tunnel representing a section of a smooth cable and a power transmission line arranged in a grouped configuration.

There are different types of classifications of the flow around twin cylinders, which depends on the distance between the two cylinders (spacing ratio) and flow direction. When the horizontal normalized spacing ratio (S/D), where S is the horizontal distance between the centerlines of cylinders and D is the diameter of the cylinder, is less than two, both cylinders behave as single combined cylinder while for large spacing ratios both cylinders act as two individual single cylinders (He et al. 2018). Over the past decades, the flow characteristics of tandem cylinders have been studied by using either wind tunnel tests or numerical simulations to measure the static or dynamic forces. Arie et al. (1983) measured the aerodynamic forces of tandem circular cylinders by conducting wind tunnel experiments and concluded that the properties of the downstream cylinder is independent of the upstream one for spacing ratios greater than 10. Lin et al.

ISSN: 1226-6116 (Print), 1598-6225 (Online)

(2002) used this technique for tandem cylinders with spacing ratios from 1.15 to 5.1 and observed the Kelvin-Helmholtz vortices at the spacing ratio of 4. Jenkins et al. (2006) applied two-dimensional PIV to capture the flow field over twin cylinders with spacing ratios of 1.4 and 3.7 and showed that wakes are more organized for a spacing ratio of 3.7 than those of spacing ratio of 1.4. Liu et al. (2008) studied the flow characteristics over equal and unequal twin cylinders to calculate the aerodynamic coefficients in smooth and turbulent flows. The results showed that the wake galloping might happen for spacing ratios from 3 to 5. Kim et al. (2009a, 2009b) carried out the dynamic wind tunnel tests for spacing ratios from 0.1 to 3.2 and showed that the dynamic response of upstream and downstream cylinders are more dependent on spacing ratios less than 2.7.

Korkischko and Meneghini (2010) conducted the dynamic tests through stereoscopic digital particle image velocimetry (SDPIV) to capture the flow around tandem cylinders with spacing ratios from 2 to 6. Moreover, they studied the effect of strakes on vibration mitigation and concluded that it suppresses the motion of the downstream cylinder for some cases. Assi et al. (2010a) performed a series of water tunnel tests to capture the wake-induced vibration of twin cylinders and proposed several practical solutions to suppress the vibration. Assi et al. (2010b) investigated the characteristics of flow around tandem circular cylinders by performing wind tunnel tests and discussed the mechanism of wake-induced vibration based on their results. They concluded that the wake-induced vibration of the downstream cylinder is mitigated if the unsteady vortices of the upstream cylinder are suppressed. Huera-Huarte and Gharib (2011) studied the flow-induced vibration of side-by-side circular cylinders with an aspect ratio of 5 by performing wind tunnel experiments while one cylinder was free or fixed. They reported vibration amplitude, frequencies, and phase synchronization. The results indicated that fixing one of the cylinders is only important when they vibrate out-of-phase. Alam and Meyer (2013) measured the vibration of twin cylinders for staggered arrangement and classified the flow around twin cylinders into seven regimes. Armin et al. (2018) studied the wake-induced galloping of tandem circular cylinders for spacing ratios of 3.5-20 at Reynolds numbers ranging from 8.7×10^3 to 5.2×10^4 . They used the water tunnel to measure the dynamic response of the downstream cylinder at different spacing ratios to determine the interaction of vortex shedding generated by the upstream and downstream cylinders. Particle image velocimetry (PIV) technique is another method that has been used to investigate this phenomenon.

Palau-Salvador *et al.* (2008) conducted a numerical simulation using the large eddy simulation (LES) turbulence model to study the flow behavior and validated the results with experimental data. Carmo *et al.* (2010) applied direct stability analysis and numerical simulation to investigate the secondary instabilities of the flow in the wake of tandem cylinders for spacing ratios of 1.2 to 10 and explored the dependency of critical Reynolds number and flow separation. Dehkordi *et al.* (2011) measured the

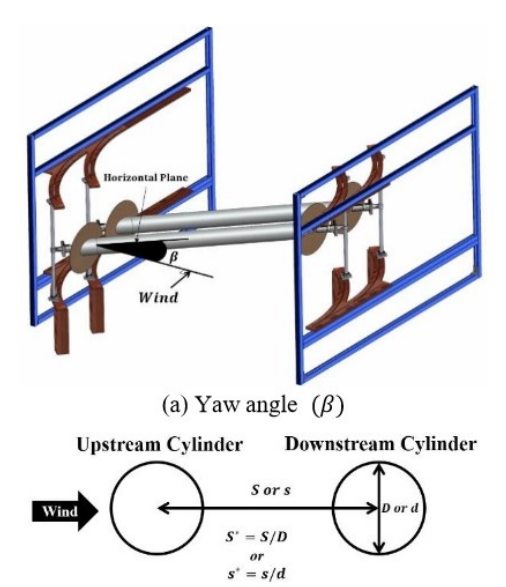
Strouhal number, drag and lift coefficients of tandem circular cylinders by conducting a two-dimensional numerical simulation in laminar and turbulent flows. They carried out the simulations for Reynolds numbers ranging from 100 to 22,000 and validated the obtained results with experimental data. Lam et al. (2012) simulated the flow field over yawed plain and wavy cylinders in a tandem arrangement for spacing ratios from 1.5 to 5.5 by conducting three-dimensional large eddy simulation (LES) at yaw angles of 0° and 30°. They compared the results of Strouhal number for plain and wavy cylinders at different yaw angles and concluded that the spacing ratio of 3.5 is the critical value for the wavy cylinders. Nguyen et al. (2018) simulated the flow field over twin cylinders using the hybrid detached eddy simulation (DES) turbulence model and measured the force component, pressure distribution, and dynamic response of cylinders at subcritical Reynolds number (Re) ranging from 10⁴ and 10⁵ and spacing ratio of 4 to 5. The results showed that the Reynolds number has a strong effect on wake galloping, and the numerical simulations accurately predicted the increase of response frequency with increasing wind speed.

Apart from past studies on aerodynamic instability of single cables because of vortex-induced vibration, rainwind-induced vibration, and galloping (Li et al. 2016, Gorski 2016, An et al., 2016, Burlina et al. 2018, Shen et al. 2018), there were studies on tandem cables especially in non-yawed arrangement to capture the wake-induced instability of structural cables and power transmission lines. The wake-induced galloping of cables usually occurs for moderate spacing ratios (Tokoro et al. 2000). For tandem smooth cables, the only criterion describing the onset of wake galloping instability has been proposed by FHWA (Kumarasena et al. 2007). The galloping is triggered when the wind speed exceeds $U_{cr} = cf_n D\sqrt{Sc}$, where c is a constant dependent on inter-cable spacing and orientation, f_n is the natural frequency, D is the cable diameter, and Sc is the Scruton number. The constant number of c has the values of 25 and 80 for horizontal and vertical spacing ratios of 2-6 and 10, respectively (Kumarasena et al. 2007). Gawronski (1978) simulated the wake-induced vibration of bundle power transmission lines and smooth cables and indicated that wake galloping occurs at higher wind speed by increasing the spacing ratio. The comparison between twin smooth cables and conductors demonstrates that the galloping instability occurs in higher wind speeds for smooth cables compared to power transmission lines. Yoshimura et al. (1993) conducted wind tunnel experiments to test a new mitigation device for suppressing the wake galloping of two parallel cables. They did the experiments for staggered configuration at different wind incident angles and concluded that the critical wind incident angle is 5°. Tokoro et al. (2000) studied the aerodynamics of tandem cables by performing a series of wind tunnel tests for different spacing ratios (normalized distance between cables) ranging from 4.3 to 8.7 to study the wake galloping of parallel cables. They concluded that the smooth cables are stable for spacing ratios greater than 6.5 and showed that the vibration of the leeward (downstream) cable depends on both reduced velocity and

Reynolds number (Re). Li et al. (2013) conducted a study on wake-cable galloping using wind tunnel experiments to study the three-dimensionality of flow and measured the wind response. They also showed the effectiveness of attaching flexible and rigid connections between the cables located at their mid-span and quarter-span positions. Kim and Kim (2014) performed the wind tunnel test to measure the wake-induced vibration of smooth cylinders and found that the vibration amplitude becomes larger for smaller spacing ratios. They observed random vibration only for the large spacing ratios due to less interaction between vortex shedding of the upstream cylinder and downstream one. Acampora et al. (2014) carried out full-scale monitoring and wind tunnel test on the arrangement of twin cables for the Øresund Bridge to extract the aerodynamic damping and stiffness using the Eigenvalue Realization Algorithm (ERA).

Qin et al. (2017) measured the flow-induced vibration of the downstream cylinder in a tandem arrangement for spacing ratios ranging from 1 to 5.5 while changing the diameter of the upstream cylinder. They presented the vibration, frequency response, surface pressure, and shedding frequencies through using the laser vibrometer, hot-wire, pressure scanner, and particle image velocimetry. Furthermore, they captured six distinct flow regimes and discussed the dependency of cylinder vibration on spacing and diameter ratios. The natural frequency ratio of upstream and downstream cylinders is another important parameter influencing the wake-induced vibration, and this parameter was studied by Qin et al. (2018). They carried out a series of experiments for six different natural frequency ratios $(f_n^* = f_{n,u}/f_{n,d})$ of 0.6, 0.8, 1.0, 1.2, 1.4, and 1.6 while the spacing ratio was tested for 1.5 and 2.0. They observed a jump in the response of the downstream cylinder at critical reduced velocity. They concluded that the increase and reduction of vibration of the downstream cylinder highly depend on the natural frequencies of cylinders. Moreover, they discussed the influence of the natural frequency ratio on vortex-shedding frequency through a comprehensive analysis. He et al. (2018) studied the wake-induced galloping of tandem cables by wind tunnel measurement. They observed a large-amplitude vibration for downstream cable and showed the tendency of an increase in vibration frequency with increasing wind speed. Qin et al. (2019) studied the galloping of the tandem cylinder by changing the reduced velocity from 3.8 to 47.8 and spacing ratios ranging from 1.2 to 6. They demonstrated the impact of alternating reattachment, detachment, rolling up, and shedding of upper and lower gap shear layers on the flowinduced vibration of the downstream cylinder.

This paper focuses on the measurement of drag and lift, Strouhal number, and surface pressure distribution of yawed cylinders in a tandem arrangement for different spacing ratios at yaw angles ranging from 0° to 45°. This study would provide some insight into a better understanding of wake-induced loads and galloping problem of bundled cables. According to the past studies, the critical spacing ratio of smooth and grooved cylinders for the downstream cylinder experiencing the wake-induced vibration is reported as ranging from 4 to 6 (Tokoro *et al.* 2000) and 10



(b) Description of spacing ratio (S^* or s^*)

Fig. 1 Test setup and definitions of yaw angle (β) and spacing ratio $(S^* = \frac{s}{D} \text{ or } s^* = \frac{s}{d})$ for tandem cylinders

to 20 (Lilien and Snegovski 2004), respectively. This led us to select this range of spacing ratios for the present study involving yawed cables. For this purpose, a series of static wind tunnel experiments were performed to study the flow characteristics of tandem circular cylinders with smooth and grooved surfaces representing the flow over tandem smooth cables and conductors. Additionally, the coherence coefficient of the downstream cylinder was reported to reveal the dependency of the measured data on the section model's aspect ratio (length/diameter).

2. Wind tunnel model setup

In this study, all experiments were performed in the aerodynamic test section of the AABL Wind and Gust Tunnel (2.44 m W×1.83 m H) located at Iowa State University. The maximum wind speed of this closed-circuit wind tunnel in this test section is 50 m/s, where a uniform and smooth flow with the turbulence intensity of the flow of less than 0.2% can be generated. A new setup was designed to enable the testing of yawed section models in a tandem arrangement. The aerodynamic forces and surface pressure distributions of both yawed cylinders can be measured in this setup (see Fig. 1). Additionally, parameters such as yaw angle (β) , spacing ratio $(S^* = S/D \text{ or } S^* = s/d)$, and incident vertical angle of attack can be changed for the section models in this setup. The yaw angle (β) is the angle that the axis of the cylinder makes with the plane that is normal to the wind direction, S or s is the distance between the axes of the two cylinders while D or d is the diameter of the smooth and grooved cable, respectively, and S^* or s^* is the normalized distance between the two cylinders. The yaw angle (β) and spacing ratio ($S^* = s/D$) are defined in

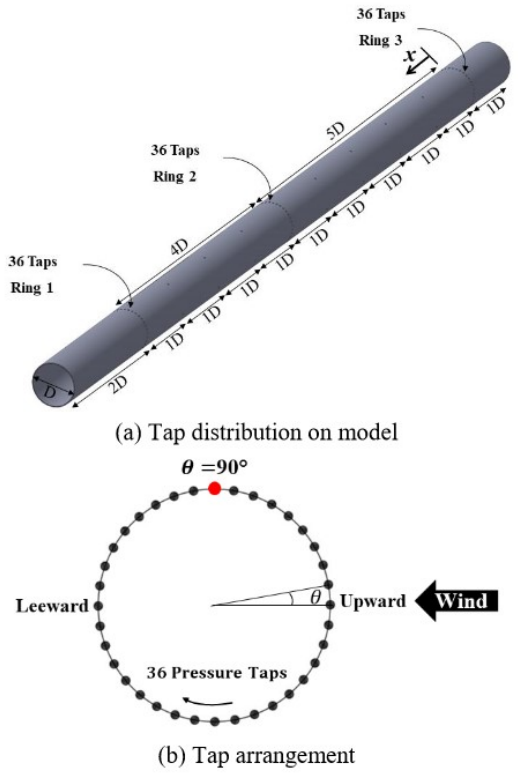


Fig. 2 Pressure taps distributed on the smooth cylinder

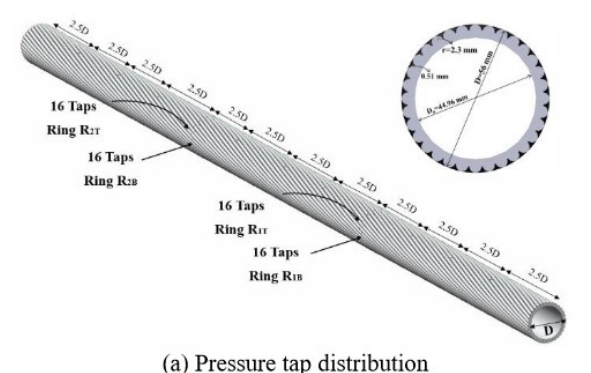
Fig. 1. For all experiments, the blockage ratio was less than 5%.

2.1 Model description: smooth cables

Two identical aluminum polished tubes or circular cylinders with a diameter (D) of 127 mm and a length (L) of 1.52 m were used as section models of the smooth cables arranged in tandem. Two end plates with circular cross section and diameter of 4D were fixed at both ends of the models to provide a two-dimensional flow over the normal and yawed cylinders. The pressure distribution of the downstream model was measured by performing static wind tunnel tests to extract the aerodynamic forces and other properties of the downstream cylinder corresponding to spacing ratios (S^*) of 4, 5, and 6 at yaw angles (β) of 0°, 15°, 30°, and 45°. As shown in Fig. 2, the model has 128 pressure taps distributed on its surface to measure the local pressure distributions at three sections and along the axis of the model. There were 36 pressure taps at the equal angular spacing of 10 degrees along each of the three rings located on the cylinder spacing by 4D or 5D distance apart and 20 other pressure taps at the equal spacing of 1D along the length of the cylinder in between the rings, seven taps each at θ =0° and 90° and 6 taps at θ =180° (see Fig. 2(a) and Fig. 2(b)). Furthermore, the aerodynamic loads were recorded by two load cells (JR3-30E12A) attached at each side of the models to verify the pressure data. Fig. 3 shows the experimental setup for tandem circular cylinders



Fig. 3 Test setup of yawed smooth cylinders in tandem arrangement



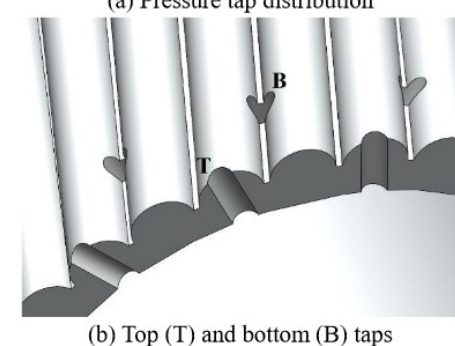


Fig. 4 Schematic of the grooved model with pressure taps

at the yaw angle of 45° and shows that the load cells and pressure transducers used for the measurements are attached to the downstream cylinder. The experiments were carried out in the uniform and smooth flow (<0.2% turbulence) at wind speeds of 5.9-22.6 m/s (Re= 9.2×10^4 to 2.67×10^5).

2.2 Model description: poser conductors

To model the surface of a high-voltage power transmission line or conductor, a grooved surface representing the helical strands of an aluminum conductor at the same scale was made by a 3D printer (Connex object 260). In this regard, 32 helical strands with a pitch of 0.762 m were designed for the two grooved cylinders, as shown in Fig. 4. The maximum diameter (d) and length of the model (l) are 56 mm and 1.52 m, respectively. Although the aspect



Fig. 5 Test setup of yawed grooved cylinders in tandem arrangement

ratio (l/d=27) was enough to avoid the edge effects, two end plates with circular cross section and diameter of 5d were fixed on two sides of the model and aligned with the flow direction to ensure two-dimensionality of the flow and avoid edge effects. For pressure measurement, 91 pressure taps were uniformly distributed on its surface to measure the local pressures. All dimensions of the grooved model and the cross section are illustrated in Fig. 4. As shown in Fig. 4(a), each model generally has four rings with 16 pressure taps at the equal angular spacing of 22.5 degrees. Since the pressure distribution on the surface of each strand may differ from the pressure in existing gap between the strands, two rings (R_{1T}, R_{2T}) were located on the top or crest of the strands, and two rings (R1B, R2B) at the bottom or trough of the valley between the strands (see Fig. b). Additionally, the surface pressure along the axis of the model was also measured at the equal spacing of 2.50d to determine the coherence of spanwise pressure distribution. The experiments were performed for spacing ratios ($s^* =$ s/d) of 10, 15, and 20 at yaw angles of 0°, 15°, 30° and 45°. The test setup of tandem grooved cylinders is shown at the yaw angle of 45° in Fig. 5.

3.3 Data acquisition

Two 64-channel pressure scanner (ZOC 33/64 Px-Scanivalve) were employed for pressure data measurement. A Scanivalve ERAD module was used to read and assimilate data from the two ZOC modules and transmit it to the computer. The precision and measurement range of ZOC are ±0.08% and -100/+350 kPa, respectively. The sampling rate and sampling time for all pressure measurements were 250 Hz and 60 s. To reduce the experimental error, three data sets for each test were recorded with LabVIEW (National Instruments) software, and the average values of results extracted from the three data sets were reported in the results. The diameter of the vinyl tubing that was used for pressure measurement was 0.86 mm while its length was a variable to cover the farthest to the nearest pressure tap on the models. To minimize the error in the dynamic pressure measurements due to the tubing length without correction, both ZOCs were placed inside the wind tunnel near the model (see Figs. 3 and 5) and the tubing frequency response was estimated using a

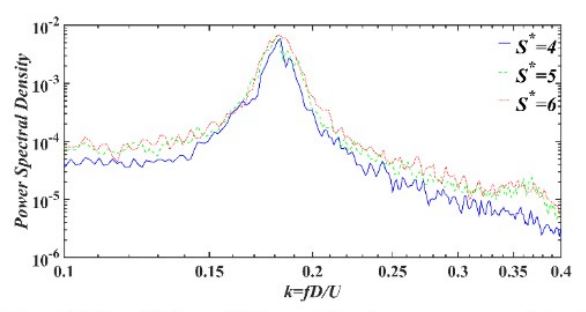


Fig. 6 PSD of lift coefficient of the downstream model of two smooth tandem cylinders at $\beta = 0^{\circ}$ and

U = 18.5 m/s

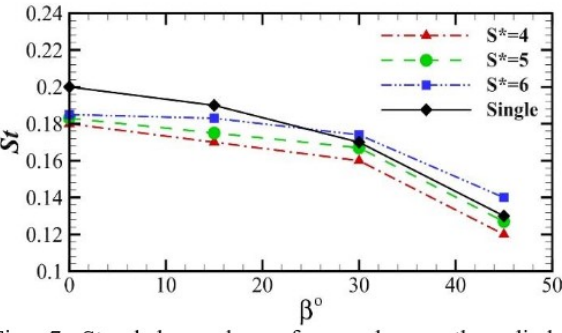


Fig. 7 Strouhal number of yawed smooth cylinder (downstream) in the tandem arrangement of two smooth cylinders and a single cylinder

software (D.R.O.P. Tubes, Australian Wind Engineering Society) for an average tubing length of 0.90 m and tubing diameter of 0.86 mm. The maximum frequency without any significant distortion in the PSD of pressure (<10%) was estimated as 75 Hz which corresponds to a maximum reduced frequency of 0.51 and 0.23 for the smooth cable and grooved cable, respectively, for a mean wind speed of 18.5m/s that was later used in the analysis of fluctuating pressures. Aerodynamic loads were also measured by two six-component load cells (JR3s) that were perpendicularly attached at both ends of the model to record the aerodynamic forces and moments along the three axes. The JR3 has a precision of \pm 0.25% of its load capacity with a measurement range of ±40 N. The sampling frequency and the sampling time for the JR3 were 500 Hz and 60 s, respectively.

There are two major sources of error or uncertainty in any experimental study. The error from the first source depends on the precision of the instruments used for the experiment and is quantifiable. The second one is the systematic and random error that originates from the experimental setup and environmental conditions, and hence is difficult to assess. The second error was minimized here by averaging over multiple data runs. The error from the instruments in each of the measured parameters, aerodynamic pressure and force coefficients, can be estimated from the precision of the instruments that were used in this study. The precision of the pressure scanner (Scanivalve® ZOC 33/64) is ±0.08% of the measured

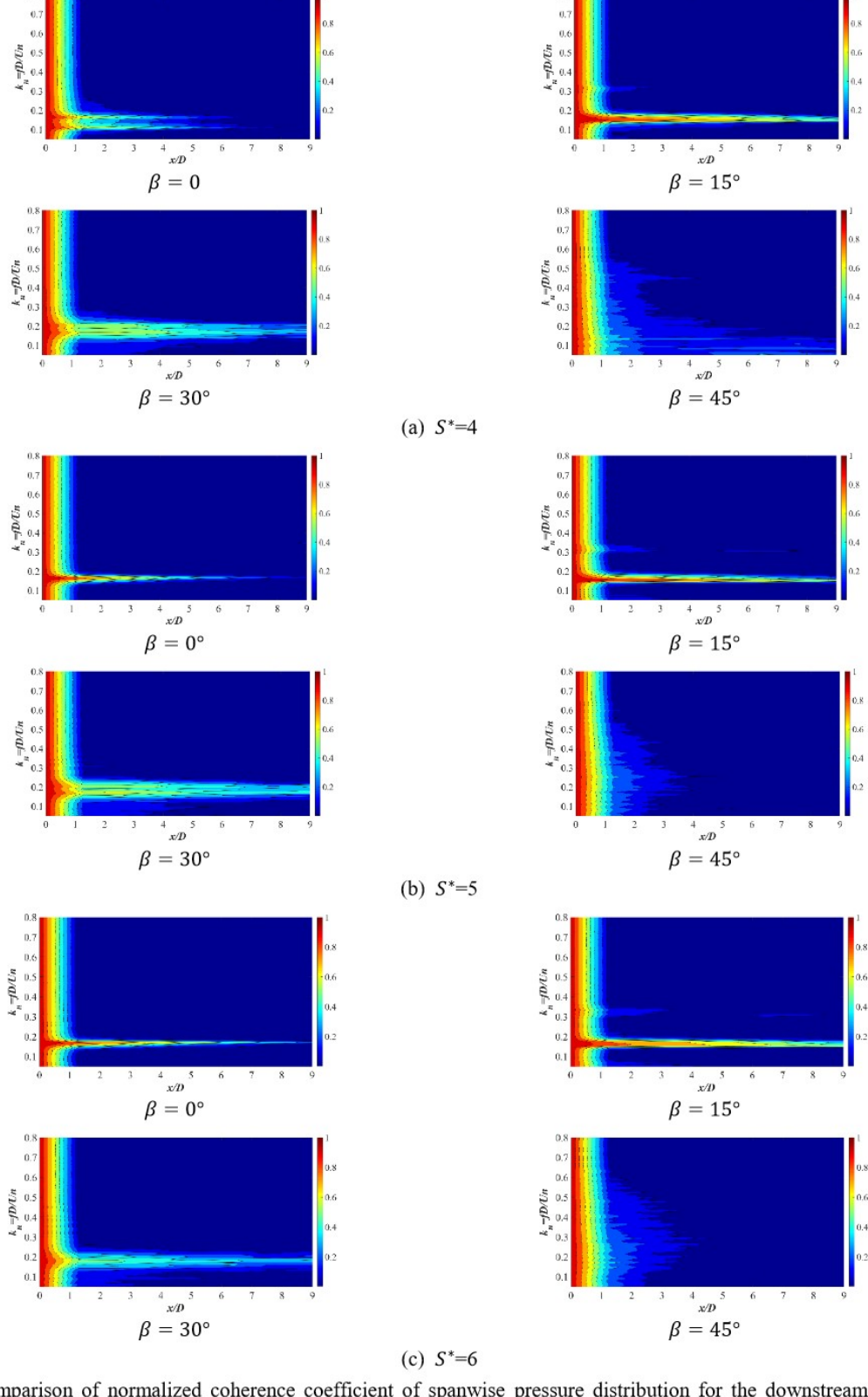


Fig. 8 Comparison of normalized coherence coefficient of spanwise pressure distribution for the downstream cylinder at $\theta = +90^{\circ}$ for two cylinders (smooth) in tandem arrangement

6 of 15

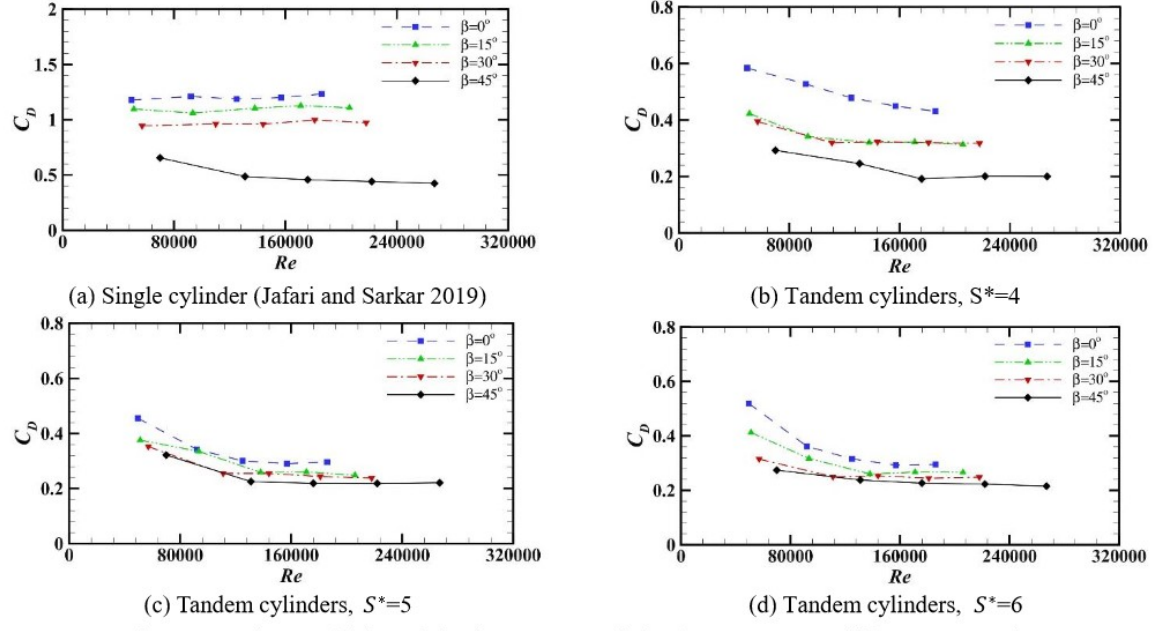


Fig. 9 Mean drag coefficient of the downstream cylinder for $S^*=4, 5, 6$ at different yaw angles

pressure. Based on this precision and estimated error in measurement of mean wind speed, the maximum error in the mean pressure coefficient (Cp) is estimated to be 0.68%.

4. Results and discussion

4.1 Tandem smooth cylinders

In this study, the Strouhal number of the yawed cylinder is defined as $St(\beta) = f_s D/U$, where β is yaw angle as explained earlier, f_s is the frequency of vortex shedding, D is the diameter of the cylinder, and U is the mean wind speed. The Strouhal number of the downstream cylinder was calculated from the power spectral density (PSD) of fluctuating lift coefficient for different spacing ratios of 4, 5, and 6 at yaw angles from 0° to 45°. In Fig. 6, the PSD of lift coefficient of the downstream cylinder versus reduced frequency (k = fD/U) is plotted for different spacing ratios at a wind speed of 18.5 m/s, and the Strouhal number is reported based on the peak value of the PSD. Since the Strouhal number was almost constant at subcritical Reynolds number, the average value of the Strouhal number of the downstream cylinder is plotted in Fig. 7 for different yaw angles and spacing ratios. As shown in Fig. 7, the Strouhal number of the downstream cylinder in a tandem arrangement is less than the Strouhal number of a single cylinder (Jafari and Sarkar, 2019) that is in good agreement with past studies for non-yawed cylinders in the tandem arrangement (Xu and Zhou, 2004). Furthermore, the results indicate that the Strouhal number slightly increases with the spacing ratio at a given yaw angle, but more datasets for other spacing ratios are required to accurately prove the dependency of Strouhal number on the spacing ratio.

The correlation coefficient is another important parameter to characterize the aerodynamic forces of normal and yawed circular cylinders (Cheng and Tanaka 2005). The spanwise behavior of flow around the downstream cylinder was studied by finding the normalized coherence coefficient varying from 0 to 1 from the pressure distribution along its axis. The magnitude of the squared coherence coefficient (γ^2), which is defined in Eq.(1), was calculated from pressure data collected at 10 spanwise locations with equal spacing of D placed at the top of the cylinder ($\theta = +90^{\circ}$) along the cylinder axis.

$$C_{ij}(\Delta x, f) = \frac{\left|S_{ij}(\Delta x, f)\right|^2}{S_{ii}(x, f)S_{ij}(x, f)} \tag{1}$$

where C_{ij} is the normalized spanwise coherence coefficient ranging from 0 to 1, S_{ij} is the cross-power spectral density, S_{ii} and S_{jj} are the auto-power spectral density of pressure data, i and j are the locations of pressure taps ranging from 1 to 9 (smooth cylinder) and 25 (grooved cylinder) distributed along the cylinder axis separated by distance Δx . Fig. 8 shows the contour plot of the normalized coherence coefficient of pressure data in the spanwise direction for different spacing ratios and normal reduced frequencies $(k_n = fD/U_n)$, where $U_n =$ $Ucos(\beta)$), at various yaw angles. As shown in Fig. 8, the normalized coherence coefficient of the non-yawed cylinder $(\beta = 0^{\circ})$ becomes almost zero for a separation ratio $(\Delta x/D)$ greater than 9, which means the captured data in spanwise direction is uncorrelated for aspect ratios greater than 10. Furthermore, the results shown in Fig. 8 indicate that the minimum aspect ratio for yawed cylinders, especially for $\beta=15^{\circ}$ and 30°, should be greater than 10 to study flow around them because of the larger correlation length. The

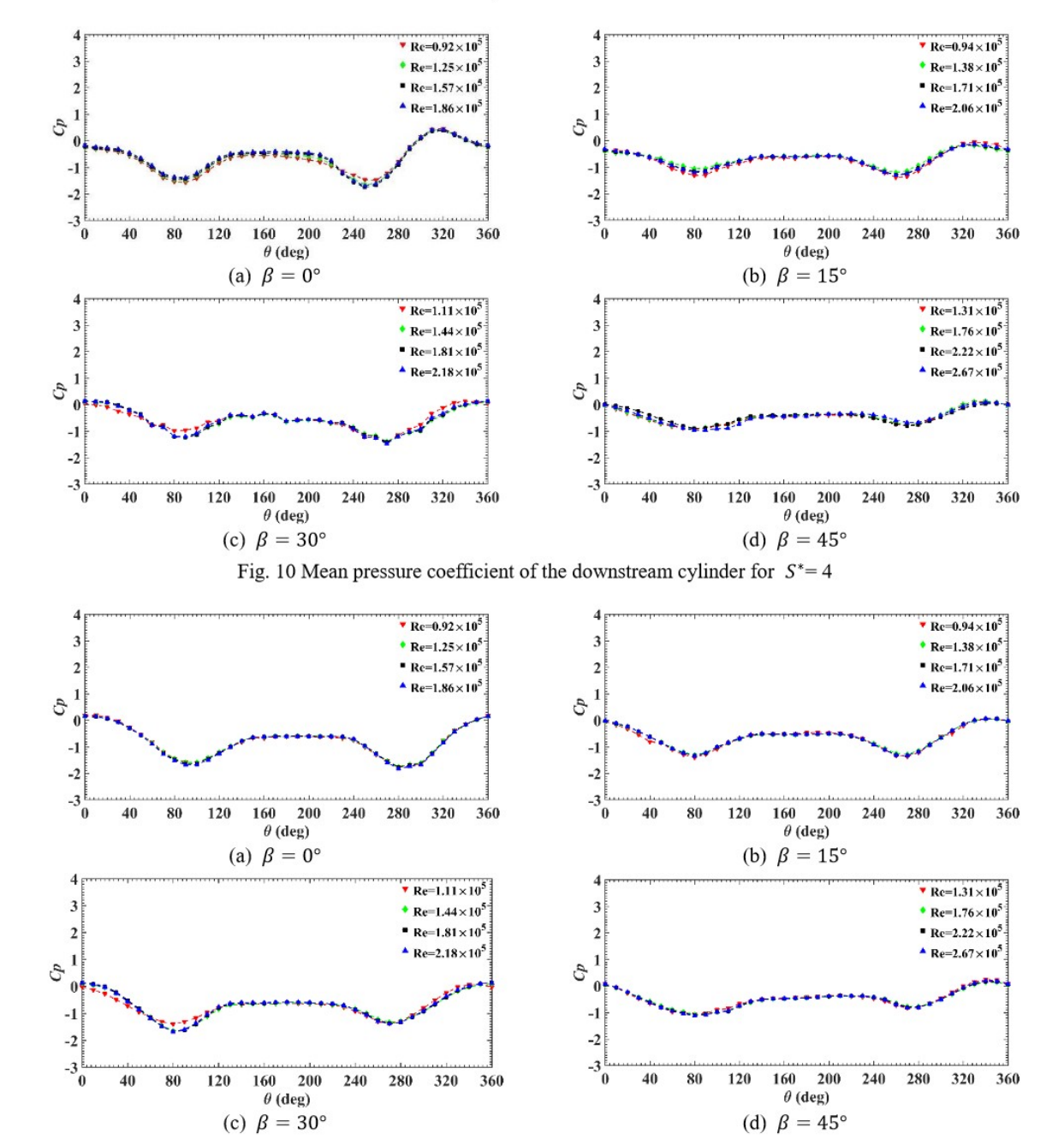


Fig. 11 Mean pressure coefficient of the downstream cylinder for $S^*=5$

comparison of spanwise coherence of pressures also demonstrates that the range of reduced frequency, which has a non-zero coherence coefficient, enlarges as yaw angle increases, and the peak of γ^2 for yaw angle of 45° is not as dominant as other yaw angles. This can be explained as the effect of axial flow behind the cylinder that mitigates the strength of vortex shedding as the yaw angle increases due to the interaction of vortex shedding and axial flow.

The drag coefficient $(C_D(\beta) = F_D/0.5\rho U^2DL)$ of the downstream cylinder, which is calculated from the pressure

distribution, is plotted for $S^* = 4$, 5, and 6 at different yaw angles in Figs. 9(b) - 9(c). The results show that C_D reduces with increasing yaw angle at a given Reynolds number. Additionally, the drag coefficient decreases at each yaw angle as the Reynolds number increases, and this reduction is more for smaller yaw angle at a given spacing ratio. It seems that the drag reduction for the downstream cylinder in a tandem arrangement is indirectly dependent on the Reynolds number and yaw angle that influence the flow around the upstream cylinder and hence its wake

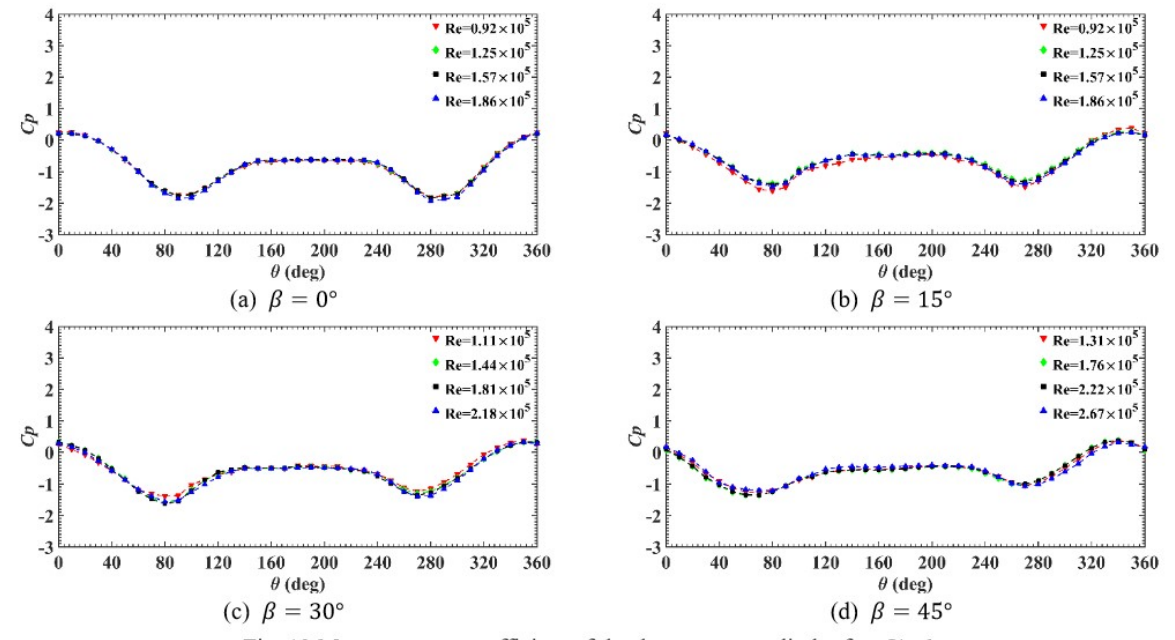


Fig. 12 Mean pressure coefficient of the downstream cylinder for $S^*=6$

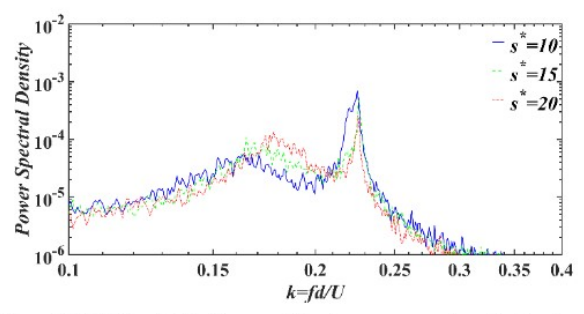


Fig. 13 PSD of lift force of tandem grooved cylinder for $s^*=10, 15, 20$ at $\beta=0^\circ$ and U=18.5 m/s

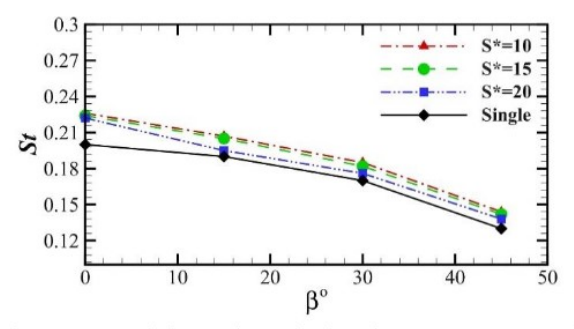


Fig. 14 Strouhal number of the downstream grooved cylinder and single smooth cylinder

characteristics, which govern the flow and surface pressure distribution around the downstream cylinder as a function of the normalized spacing between the two cylinders. The lift coefficient was found to be zero that is consistent with past studies for non-yawed cylinders in the tandem arrangement (Alam and Meyer 2013).

In Figs. 10 - 12, the mean pressure coefficient distributions around the downstream cylinder are plotted for $S^* = 4$, 5, 6 at Reynolds numbers varying from 9.2×10^4 to 2.67×10⁵. It should be noted that the pressure distributions plotted hereafter are the mean values calculated from the time histories of pressure data. The experimental results show that the reattachment point for $S^*=4$ is located at 320° or -40° (lower surface) as circled in Fig. 10(a) that is consistent with a past study (Sharman et al. 2005) and validates the present pressure measurement. Past studies show that the reattachment point(s) mainly depends on the spacing ratio and Reynolds number. These figures indicate that the pressure distribution does not change for the Reynolds number studied here. In addition, it can be seen that the absolute value of pressure drop occurring at separation points becomes less with increasing yaw angle. The pressure distribution also shows that the location of separation point changes with spacing ration due to the influence of the upstream cylinder.

4.2 Tandem grooved cylinders

Since the comparison of the mean pressure distribution on top and bottom surfaces of the downstream grooved cylinder showed an insignificant difference, the pressure data of the top surface at each ring of taps were used to calculate the properties of the downstream model. The Strouhal number of the downstream cylinder was calculated from the PSD of the lift coefficient versus reduced frequency (k = fd/U) that is plotted for different spacing ratios in Fig. 13. This figure shows a peak in the PSD for each case with the same magnitude indicating that the strength of vortex shedding is approximately similar for yawed cylinders at all spacing ratios. In Fig. 14, the

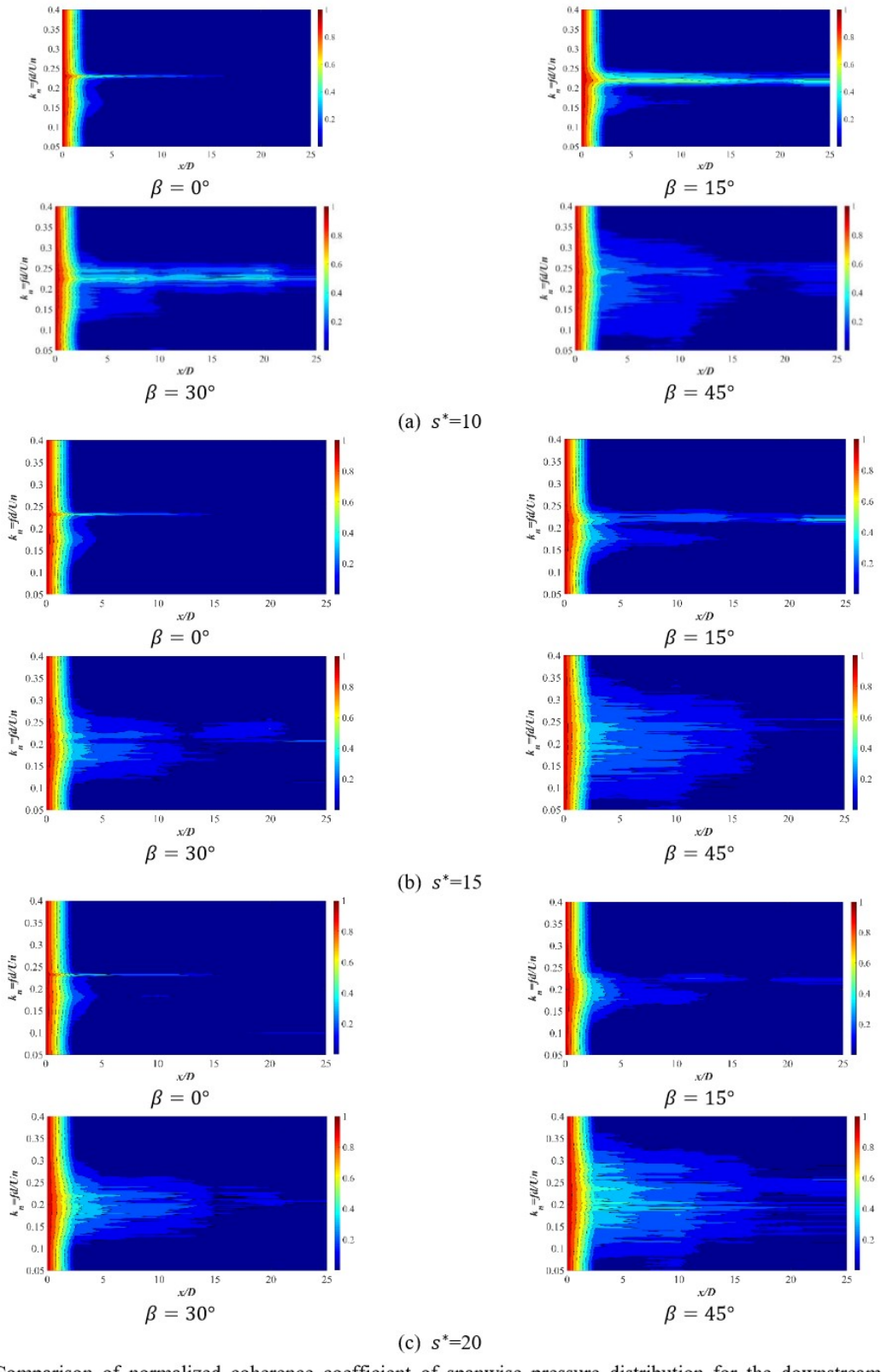


Fig. 15 Comparison of normalized coherence coefficient of spanwise pressure distribution for the downstream grooved cylinder at $\theta = +90^{\circ}$ for two cylinders (grooved) in a tandem arrangement

10 of 15

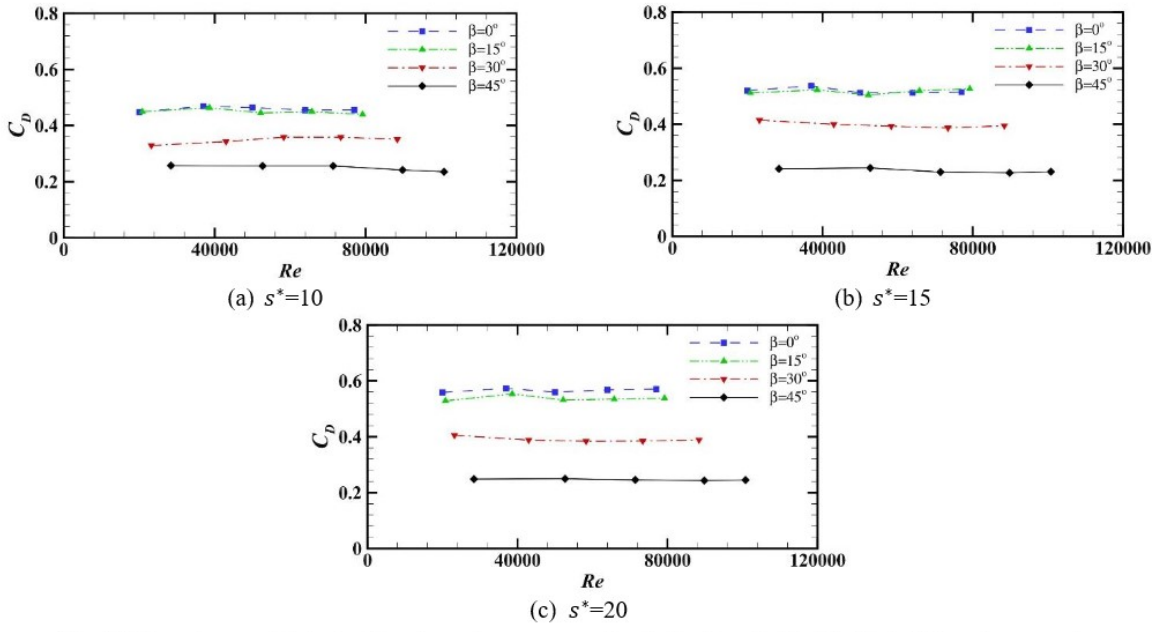


Fig. 16 Mean drag coefficient of the downstream grooved cylinder for s*=10, 15, 20 at different yaw angles

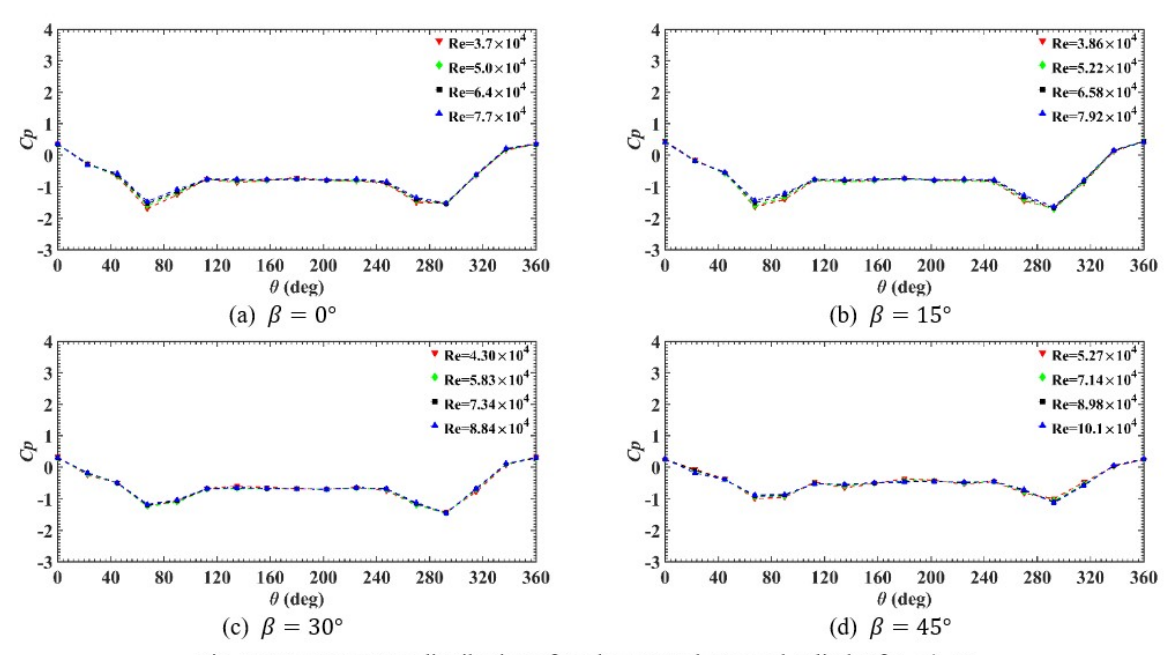


Fig. 17 Mean pressure distribution of tandem yawed grooved cylinder for $s^*=10$

Strouhal numbers for the downstream yawed cylinder are shown for different spacing ratios. From the plots in Fig. 14, it can be concluded that the Strouhal number varies slightly with the spacing ratio, but it is not significant enough that means the effect of the spacing ratio of 10 or higher on the Strouhal number for the downstream cylinder is negligible across different yaw angles.

The normalized coherence coefficient of a grooved cylinder was calculated from 25 pressure taps distributed along its axis for different spacing ratios and yaw angles.

The results, which are shown in Fig. 15 as the contour plot of normalized coherence coefficient versus normal reduced frequency $(k_n = fd/U_n)$, helps to understand the flow behavior over the grooved cylinder in the spanwise direction. According to the obtained results, there is no dependency beyond the separation ratio $(\Delta x/d)$ of 10 for the non-yawed cylinder that is similar to the behavior of smooth tandem cylinders. However, the normalized coherence coefficient of the yawed cylinder becomes nearly zero for separation ratios or aspect ratios greater than 20.

11 of 15 6/24/2020, 8:04 PM

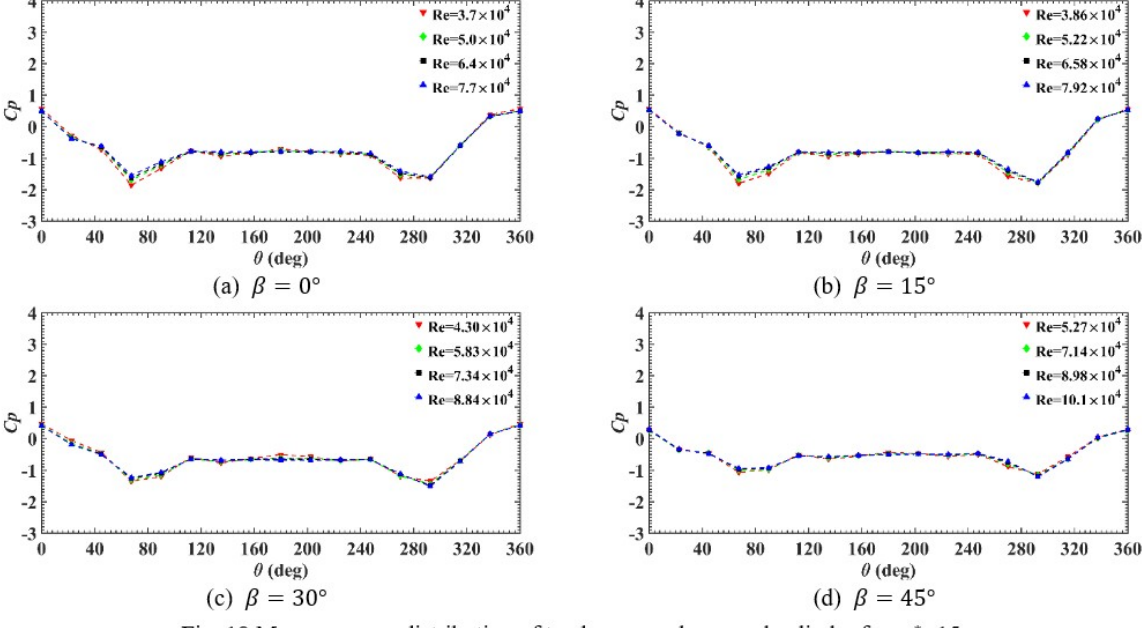


Fig. 18 Mean pressure distribution of tandem yawed grooved cylinder for s*=15

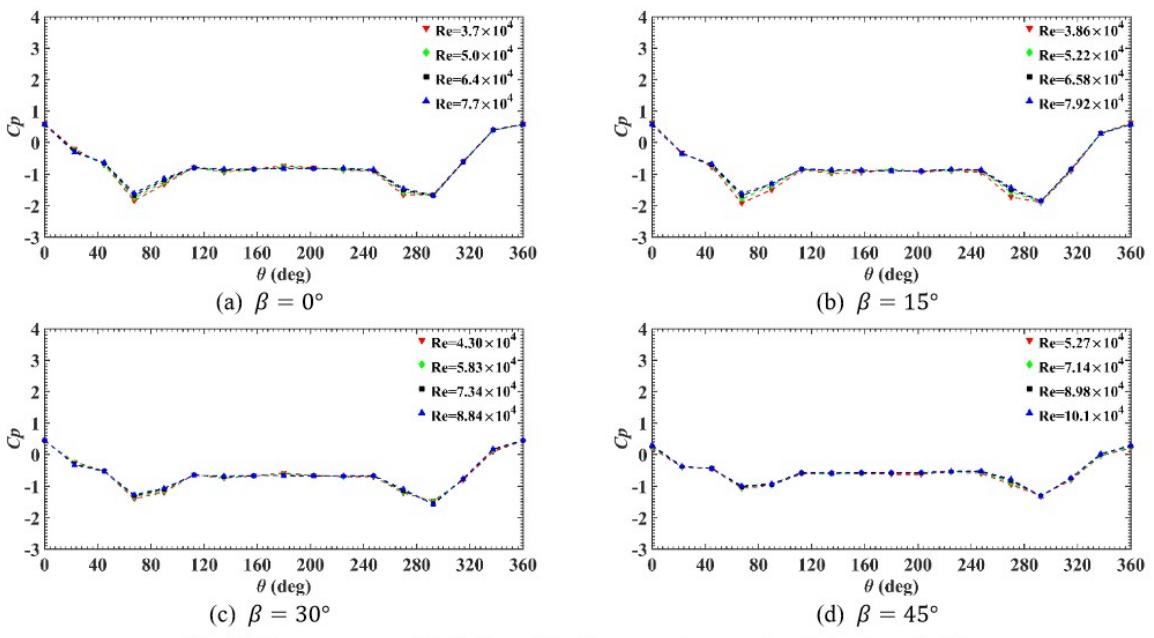


Fig. 19 Mean pressure distribution of tandem yawed grooved cylinder for $s^*=20$

For larger yaw angles, the results of the coherence coefficient indicate that the dependency of data in spanwise direction occurs in the wider range of reduced frequency compared with the results of zero yaw angle that may be due to interaction between vortex shedding and axial flow.

The drag coefficient is shown for spacing ratios (s^*) of 10, 15, and 20 in Fig. 16. The spacing ratios of smooth and grooved cylinders were chosen based on the critical spacing ratios reported in past studies for smooth cables and power transmission lines. This selection was made to investigate

the loads on tandem structural cables in critical flow regimes. The results show that the drag coefficient reduces at larger yaw angles, which is consistent with the results identified for a smooth cylinder. Furthermore, the drag coefficient for larger spacing ratios increases at a given Reynolds number and yaw angle while there is no variation in the drag coefficient at a given yaw angle and spacing ratio. Additionally, the results show that the mean lift is zero for all cases of Reynolds number tested.

The mean pressure coefficient corresponding to the

surface of the grooved cylinder is plotted for the Reynolds numbers of $3.7 \times 10^4 - 1.01 \times 10^5$ in Figs. 17-19. Although the results indicate that the mean pressure around a grooved cylinder is almost symmetric, there is a slight difference in pressure distribution between the top and bottom surfaces, which can be due to the helical strands or the resolution of pressure taps.

5. Conclusions

Inclined cables have frequently shown moderate- to large-amplitude vibration due to wind excitation that causes damage. This paper primarily studies the wind-induced load characteristics of smooth and grooved cylinders placed in the wake of another identified cylinder representing section models of smooth cables used, for example, stay-cables in bridges, and grooved cables used as helically-wound conductors in power transmission lines. However, the application of this study extends beyond structural cables and power-line conductors. In this study, the pressure measurement was conducted on the downstream cylinder for two parallel cylinders in a tandem arrangement by performing wind tunnel experiments in static conditions. The wind tunnel tests were conducted for different yaw angles and spacing ratios (normalized distance between the cylinders) for a range of Reynolds number (5×104 to 2.67×10^5 for smooth cable and 2×10^4 to 1.01×10^5 for grooved cable). For this purpose, two polished tubes with an aspect ratio (length to diameter) of 12, and two grooved cylinders with an aspect ratio of 27, as made by a 3D printer, were employed to capture the surface pressures on the cylinder at yaw angles of 0°, 15°, 30°, and 45°. The pressure data were recorded by the pressure taps that were distributed circumferentially along three separate rings and along the axis of the cylinder to investigate the flow behavior around the cylinder and its spanwise direction. The Strouhal number and drag coefficient were calculated for different spacing ratios and yaw angles. For both models with smooth and grooved surfaces, the results indicate that the Strouhal number of a yawed cylinder is smaller than the normal case at a given Reynolds number while the Strouhal number of the downstream cylinder is smaller than the Strouhal number of a single cylinder. Furthermore, the drag coefficient of a grooved cylinder is almost constant in the range of Reynolds number (2.0×10⁴ -1.01×10⁵) tested in this study, while a drag reduction was observed for the smooth cylinder with increasing Reynolds number. The spanwise flow behavior of the cylinder was investigated by showing the contour plots of normalized coherence coefficients that were identified from spanwise pressure distribution. For all spacing ratios, the normalized coherence coefficient of the non-yawed cylinder ($\beta = 0^{\circ}$) becomes close to zero beyond the aspect ratio of 9. Therefore, the obtained results indicate that the minimum aspect ratio for yawed cases should be greater than 10 to capture the uncorrelated data. Furthermore, comparison of results shows that the range of reduced frequency with nonzero coherence coefficient increases as yaw angle increases, and the peak of the coherence coefficient for yaw angle of 45° is not as dominant as other yaw angles indicating either absence or reduced strength of vortex shedding. This phenomenon can be explained by the effect of axial flow behind the cylinder that increases in magnitude with increasing yaw angle and helps to reduce the strength of vortex shedding from the cylinder through its interaction with the vortices shed alternatively from the opposite sides of the cylinder.

Acknowledgements

The authors gratefully thank the U.S. National Science Foundation (NSF) for financially supporting this project by the research grant CMMI-1537917.

References

- Acampora, A., Macdonald, J.H.G., Georgakis, C.T. and Nikitas, N. (2014), "Identification of aeroelastic forces and static drag coefficients of a twin cable bridge stay from full-scale ambient vibration measurements", J. Wind Eng. Ind. Aerod., 124, 90-98. https://doi.org/10.1016/j.jweia.2013.10.009.
- Alam, M.M. (2014), "The aerodynamics of a cylinder submerged in the wake of another", *J. Fluids Struct.*, **51**, 393-400. https://doi.org/10.1016/j.jfluidstructs.2014.08.003.
- Alam, M.M. and Meyer, J.P. (2013), "Global aerodynamic instability of twin cylinders in cross flow", J. Fluids Struct., 41, 135-145. https://doi.org/10.1016/j.jfluidstructs.2013.03.007.
- Alam, M.M., Moriya, M., Takai, K. and Sakamoto, H. (2003), "Fluctuating fluid forces acting on two circular cylinders in a tandem arrangement at a subcritical Reynolds number", J. Wind Eng. Ind. Aerod, 91(1-2), 139-154. https://doi.org/10.1016/S0167-6105(02)00341-0.
- An, Y., Wang, C., Li, S. and Wang, D. (2016), "Galloping of steepled main cables in long-span suspension bridges during construction", Wind Struct., 23(6), 595-613. https://doi.org/10.1016/S0167-6105(02)00341-0.
- Arie, M., Kiya, M., Moriya, M. and Mori, H. (1983), "Pressure fluctuations on the surface of two circular cylinders in tandem arrangement", J. Fluids Eng., 105, 161-166. https://doi.org/10.1115/1.3240956.
- Armin, M., Khorasanchi, M. and Day, S. (2018), "Wake interference of two identical oscillating cylinders in tandem: An experimental study", *Ocean Eng.*, 166, 311-323. https://doi.org/10.1016/j.oceaneng.2018.08.012.
- Assi, G.R.S., Bearman, P.W., Kitney, N. and Tognarelli, M.A. (2010a), "Suppression of wake-induced vibration of tandem cylinders with free-to-rotate control plates", *J. Fluids Struct.*, 26(7-8), 1045-1057. https://doi.org/10.1016/j.jfluidstructs.2010.08.004.
- Assi, G.R.S., Bearman, P.W. and Meneghini, J.R. (2010b), "On the wake-induced vibration of tandem circular cylinders: The vortex interaction excitation mechanism", *J. Fluid Mech.*, 661, 365-401. https://doi.org/10.1017/S0022112010003095.
- Braun, A.L. and Awruch, A.M. (2005), "Aerodynamic and aeroelastic analysis of bundled cables by numerical simulation", J. Sound Vib., 284(1-2), 51-73. https://doi.org/10.1016/j.jsv.2004.06.026.
- Burlina, C., Georgakis, C.T., Larsen, S.V. and Egger, P. (2018), "Aerodynamics and rain rivulet suppression of bridge cables with concave fillets", *Wind Struct.*, **26**(4), 253-266. https://doi.org/10.12989/was.2018.26.4.253.
- Carmo, B.S., Meneghini, J.R. and Sherwin, S.J. (2010), "Secondary instabilities in the flow around two circular cylinders in tandem", *J. Fluid Mech.*, **644**, 395-431.

13 of 15 6/24/2020, 8:04 PM

- https://doi.org/10.1017/S0022112009992473.
- Cheng, S. and Tanaka, H. (2005), "Correlation of aerodynamic forces on an inclined circular cylinder", Wind Struct., 8(2), 135-146. https://doi.org/10.12989/was.2005.8.2.135.
- Dehkordi, B.G., Moghaddam, H.S. and Jafari, H.H. (2011), "Numerical simulation of flow over two circular cylinders in tandem arrangement", *J. Hydrodyn.*, **23**(1), 114-126. https://doi.org/10.1016/S1001-6058(10)60095-9.
- Gawronski, K.E. and Hawks, R.J. (1978), "Effect of conductor geometry on bundle conductor galloping", Electr. Pow. Syst. Res., 1(3), 181-188. https://doi.org/10.1016/0378-7796(78)90022-6.
- Gorski, P., Pospíšil, S., Kuznetsov, S., Tatara, M. and Marušić, A. (2016), "Strouhal number of bridge cables with ice accretion at low flow turbulence", Wind Struct., 22(2), 253-272. http://koreascience.or.kr/article/ArticleFullRecord.jsp?cn=KJKHCF 2016 v22n2 253.
- He, X., Cai, C., Wang, Z., Jing, H. and Qin, C. (2018), "Experimental verification of the effectiveness of elastic cross-ties in suppressing wake-induced vibrations of staggered stay cables", *Eng. Struct.*, 167, 151-165. https://doi.org/10.1016/j.engstruct.2018.04.033.
- Huera-Huarte, F.J. and Gharib, M. (2011), "Flow-induced vibrations of a side-by-side arrangement of two flexible circular cylinders", *J. Fluids Struct.*, **27**(3), 354-366. https://doi.org/10.1016/j.jfluidstructs.2011.01.001.
- Jafari, M. and Sarkar, P.P. (2019), "Parameter identification of wind-induced buffeting loads and onset criteria for dry-cable galloping of yawed / inclined cables", Eng. Struct., 180, 685-699. https://doi.org/10.1016/j.engstruct.2018.11.049.
- Jenkins, L., Neuhart, D., McGinley, C., Khorrami, M. and Choudhari, M. (2006), "Measurements of unsteady wake interference between tandem cylinders", In the 36th AIAA Fluid Dynamics Conference and Exhibit., 3202.
- Kim, S., Alam, M., Sakamoto, H. and Zhou, Y. (2009a), "Flow-induced vibration of two circular cylinders in tandem arrangement. Part 2: Suppression of vibrations", J. Wind Eng. Ind. Aerod., 97(5-6), 312-319. https://doi.org/10.1016/j.jweia.2009.07.003.
- Kim, S., Alam, M., Sakamoto, H. and Zhou, Y. (2009b), "Flow-induced vibrations of two circular cylinders in tandem arrangement. Part 1: Characteristics of vibration", J. Wind Eng. Ind. Aerod., 97(5-6), 304-311. https://doi.org/10.1016/j.jweia.2009.07.004.
- Kim, S. and Kim, H.K. (2014), "Wake galloping phenomena between two parallel/unparallel cylinders", Wind Struct., 18(5), 511-528. https://doi.org/10.12989/was.2014.18.5.511.
- Korkischko, I. and Meneghini, J.R. (2010), "Experimental investigation of flow-induced vibration on isolated and tandem circular cylinders fitted with strakes", J. Fluids Struct., 26(4), 611-625. https://doi.org/10.1016/j.jfluidstructs.2010.03.001.
- Kumarasena, S., Jones, N.P., Irwin, P. and Taylor, P. (2007), "Wind induced vibration of stay cables", Missouri Deptartment of Transportation. Research, Development and Technology Division. Report No. RI-98-034.
- Lam, K., Lin, Y.F., Zou, L. and Liu, Y. (2012), "Numerical simulation of flows around two unyawed and yawed wavy cylinders in tandem arrangement", J. Fluids Struct., 28, 135-151. https://doi.org/10.1016/j.jfluidstructs.2011.08.012.
- Li, S.Y., Wu, T., Li, S.K. and Gu, M. (2016a), "Numerical study on the mitigation of rain-wind induced vibrations of stay cables with dampers", Wind Struct., 23(6), 615-639. http://dx.doi.org/10.12989/was.2016.23.6.615.
- Li, S.Y., Wu, T., Huang, T. and Chen, Z.Q. (2016b), "Aerodynamic stability of iced stay cables on cable-stayed bridge", Wind Struct., 23(3), 253-273. http://dx.doi.org/10.12989/was.2016.23.3.253.
- Li, Y., Wu, M., Chen, X., Wang, T. and Liao, H. (2013), "Wind-tunnel study of wake galloping of parallel cables on cable-stayed bridges and its suppression", *Wind Struct.*, **16**(3), 249-261. https://doi.org/10.12989/was.2013.1r6.3.249.
- Lilien, J. and Snegovski, D. (2004), "Wake-induced vibration in power

transmission line. parametric study", Flow Induc. Vib., 5. http://hdl.handle.net/2268/18268.

about:blank

- Lin, J.C., Yang, Y. and Rockwell, D. (2002), "Flow past two cylinders in tandem: Instantaneous and averaged flow structure", J. Fluids Struct., 16(8), 1059-1071. https://doi.org/10.1006/jfls.2002.0469
- Lin, Y.F., Bai, H.L., Alam, M.M., Zhang, W.G., Lam, K. (2016), "Effects of large spanwise wavelength on the wake of a sinusoidal wavy cylinder", J. Fluids Struct., 61, 392-409. https://doi.org/10.1016/j.jfluidstructs.2015.12.004.
- Liu, X., Levitan, M. and Nikitopoulos, D. (2008), "Wind tunnel tests for mean drag and lift coefficients on multiple circular cylinders arranged in-line", J. Wind Eng. Ind. Aerod., 96(6-7), 831-839.
- Matsumoto, M., Shiraishi, N., Kitazawa, M., Knisely, C., Shirato, H., Kim, Y. and Tsujii, M. (1990), "Aerodynamic behavior of inclined circular cylinders- cable aerodynamics", J. Wind Eng. Ind. Aerod., 33(1), 63-72.
- Matsumoto, M., Yagi, T., Hatsuda, H., Shima, T., Tanaka, M. and Naito, H. (2010), "Dry galloping characteristics and its mechanism of inclined/yawed cables", J. Wind Eng. Ind. Aerod., 98(6-7), 317-327. https://doi.org/10.1016/j.jweia.2009.12.001.
- Nguyen, V.T., Ronald Chan, W.H. and Nguyen, H.H. (2018), "Numerical investigation of wake induced vibrations of cylinders in tandem arrangement at subcritical Reynolds numbers", *Ocean Eng.*, 154, 341-356. https://doi.org/10.1016/j.oceaneng.2018.01.073.
- Palau-Salvador, G., Stoesser, T. and Rodi, W. (2008), "LES of the flow around two cylinders in tandem", J. Fluids Struct., 24(8), 1304-1312.
- Qin, B., Alam and M.M., Zhou, Y. (2019), "Free vibrations of two tandem elastically mounted cylinders in crossflow", J. Fluid Mech., 861, 349-381. https://doi.org/10.1017/jfm.2018.913.
- Qin, B., Alam, M.M., Ji, C., Liu, Y. and Xu, S. (2018), "Flow-induced vibrations of two cylinders of different natural frequencies", *Ocean Eng.*, 155, 189-200. https://doi.org/10.1016/j.oceaneng.2018.02.048.
- Qin, B., Alam, M.M. and Zhou, Y. (2017), "Two tandem cylinders of different diameters in cross-flow: flow-induced vibration", J. Fluid Mech., 829, 621-658. https://doi.org/10.1017/jfm.2017.510.
- Sharman, B., Lien, F.S., Davidson, L. and Norberg, C. (2005), "Numerical predictions of low Reynolds number flows over two tandem circular cylinders", *Int. J. Numer. Meth. FL.*, 47(5), 423-447. https://doi.org/10.1002/fld.812.
- Shen, X., Ma, R.J., Ge, C.X. and Hu, X.H. (2018), "Long-term monitoring of super-long stay cables on a cable-stayed bridge". Wind Struct., 27(6), 357-368. https://doi.org/10.12989/was.2018.27.6.357.
- Sumner, D. (2010), "Two circular cylinders in cross-flow: A review", J. Fluids Struct., 26(6), 849-899. https://doi.org/10.1016/j.jfluidstructs.2010.07.001.
- Tokoro, S., Komatsu, H., Nakasu, M., Mizuguchi, K. and Kasuga, A. (2000), "Study on wake-galloping employing full aeroelastic twin cable model", J. Wind Eng. Ind. Aerod., 88(2-3), 247-261. https://doi.org/10.1016/S0167-6105(00)00052-0.
- Tsutsui, T. (2012), "Experimental study on the instantaneous fluid force acting on two circular cylinders closely arranged in tandem", *J. Wind Eng. Ind. Aerod.*, **109**, 46-54. https://doi.org/10.1016/j.jweia.2012.06.005.
- Wu, C., Yan, B., Huang, G., Zhang, B., Lv, Z. and Li, Q. (2018), "Wake-induced oscillation behaviour of twin bundle conductor transmission lines, R. Soc. Open Sci., 5(6), 180011. https://doi.org/10.1098/rsos.180011.
- Wu, J., Welch, L.W., Welsh, M.C., Sheridan, J. and Walker, G.J. (1994), "Spanwise wake structures of a circular cylinder and two circular cylinders in tandem", *Int. J. Numer. Meth. Fl.*, 9(3), 299-308. https://doi.org/10.1016/0894-1777(94)90032-9.
- Wu, X., Jafari, M., Sarkar, P. and Sharma, A. (2020). "Verification of DES for flow over rigidly and elastically-mounted circular cylinders in normal and yawed flow", J. Fluids Struct., 94, 102895.

14 of 15 6/24/2020, 8:04 PM

Firefox about:blank

Wind tunnel study of wake-induced aerodynamics of parallel stay-cables and power conductor cables in a yawed flow

631

https://doi.org/10.1016/j.jfluidstructs.2020.102895.

- Xu, G. and Zhou, Y. (2004), "Strouhal numbers in the wake of two inline cylinders", Exp. Fluids, 37(2), 248-256. https://doi.org/10.1007/s00348-004-0808-0.
- Yoshimura, T., Savage, M.G., Tanaka, H. and Wakasa, T. (1993), "A device for suppressing wake galloping of stay cables for cable-stayed bridges", J. Wind Eng. Ind. Aerod., 49(1-3), 497-505. https://doi.org/10.1016/0167-6105(93)90044-O.
- Zdravkovich, M. (1987), "The effects of interference between circular cylinders in cross-flow", J. Fluids Struct., 1(2), 239-261. https://doi.org/10.1016/S0889-9746(87)90355-0.
- Zdravkovich, M. (1977), "Review of flow interference between two circular cylinders in various arrangements", J. Fluids Eng., 99(4), 618-633. https://doi.org/10.1115/1.3448871.
- Zhou, Y. and Mahbub Alam, M. (2016), "Wake of two interacting circular cylinders: A review", Int. J. Heat Fluid Flow, 62(part B), 510-537. https://doi.org/10.1016/j.ijheatfluidflow.2016.08.008.

AD

15 of 15